The CRISPR Journal
Volume 6, Number 6, 2023

DOI: 10.1089/crispr.2023.0056

The CRISPR Journal

RESEARCH ARTICLE

Engineered Antiviral Sensor Targets Infected Mosquitoes

Elena Dalla Benetta,[1,†] Adam J. López-Denman,[2,†] Hsing-Han Li,[1,†] Reem A. Masri,[1,†] Daniel J. Brogan,[1] Michelle Bui,[1] Ting Yang,[1] Ming Li,[1] Michael Dunn,[2] Melissa J. Klein,[2] Sarah Jackson,[2] Kyle Catalan,[2] Kim R. Blasdell,[2] Priscilla Tng,[3] Igor Antoshechkin,[4] Luke S. Alphey,[3,5] Prasad N. Paradkar,[2,*] and Omar S. Akbari[1,*]

Abstract

Escalating vector disease burdens pose significant global health risks, as such innovative tools for targeting mosquitoes are critical. CRISPR-Cas technologies have played a crucial role in developing powerful tools for genome manipulation in various eukaryotic organisms. Although considerable efforts have focused on utilizing class II type II CRISPR-Cas9 systems for DNA targeting, these modalities are unable to target RNA molecules, limiting their utility against RNA viruses. Recently, the Cas13 family has emerged as an efficient tool for RNA targeting; however, the application of this technique in mosquitoes, particularly *Aedes aegypti*, has yet to be fully realized. In this study, we engineered an antiviral strategy termed REAPER (vRNA Expression Activates Poisonous Effector Ribonuclease) that leverages the programmable RNA-targeting capabilities of CRISPR-Cas13 and its potent collateral activity. REAPER remains concealed within the mosquito until an infectious blood meal is uptaken. Upon target viral RNA infection, REAPER activates, triggering programmed destruction of its target arbovirus such as chikungunya. Consequently, Cas13-mediated RNA targeting significantly reduces viral replication and viral prevalence of infection, and its promiscuous collateral activity can even kill infected mosquitoes within a few days. This innovative REAPER technology adds to an arsenal of effective molecular genetic tools to combat mosquito virus transmission.

Introduction

Arboviruses are among the most widespread pathogens affecting humans, causing deadly diseases worldwide, and their geographic distribution and incidences are escalating globally due to a changing climate. RNA arboviruses belong to the families *Flaviviridae*, *Togaviridae*, and *Bunyaviridae*, and are primarily transmitted by mosquitoes.[1] More specifically, *Aedes* mosquitoes transmit numerous arboviruses, such as chikungunya (CHIKV), dengue (DENV), yellow fever (YFV), and Zika (ZIKV), which together infect hundreds of millions of people annually. Existing traditional vector control strategies have not adequately curtailed either virus transmission or the spread of mosquitoes to new habitats.[2] Therefore, novel vector-control strategies are required.

Historically, efforts to reduce viral transmission have focused on the use of chemical insecticides and the development of vaccines. However, with the rise of insecticide resistance[3] and the limited efficacy of vaccines,[4,5] there is a critical need for improved control strategies. For many arboviruses, such as DENV, ZIKV and CHIKV, vaccination efficacy is limited or under development.[6–8] For others such as yellow fever or Japanese encephalitis, vaccine availability can vary depending on several factors, including the country or region where it is needed, the demand for the vaccine, and the availability of the vaccine manufacturer.[4,5,9]

Alternatively to vaccines, several molecular tools, such as broadly neutralizing antibodies[10] and encoded miRNA arrays,[11,12] have been introduced to mosquitoes

[1]*Department of Cell and Developmental Biology, School of Biological Sciences, University of California, San Diego, La Jolla, California, USA;* [2]*CSIRO Health and Biosecurity, Australian Centre for Disease Preparedness, Geelong, Australia;* [3]*Arthropod Genetics, The Pirbright Institute, Pirbright, United Kingdom;* [4]*Division of Biology and Biological Engineering (BBE), California Institute of Technology, Pasadena, California, USA; and* [5]*Department of Biology, University of York, York, United Kingdom.*
[†]*These authors contributed equally to this study.*

*Address correspondence to: *Prasad N. Paradkar, CSIRO Health & Biosecurity, Australian Centre for Disease Preparedness, Geelong, VIC 3220, Australia*, E-mail: prasad.paradkar@csiro.au or *Omar S. Akbari, School of Biological Sciences, Department of Cell and Developmental Biology, University of California, San Diego, La Jolla, CA 92093, USA*, E-mail: oakbari@ucsd.edu

and shown to mitigate DENV and ZIKV transmission. In addition, CRISPR-Cas technologies have been engineered to control mosquito populations using the precision-guided Sterile Insect Technique[13] and confinable gene drives.[14,15] These molecular tools present great promise as vector control strategies capable of reducing viral spread by mosquitoes. However, the rapid evolution of pathogens requires the development of easily programmable technologies with direct activity against evolving and emerging infectious diseases.

Unlike traditional CRISPR technologies for insect control that target DNA and thus the mosquito vector, alternative systems that target RNA that could instead be effective against the arboviruses themselves. Cas13 is one such system that originally evolved as an RNA antiviral in prokaryotes,[16] and has emerged as programmable RNA-targeting ribonucleases.[16] The high efficiency of programmable Cas13 has been demonstrated in human cells,[17] zebrafish,[18] mice,[19] flies,[20,21] and plants,[22] but the high on-target activity is natively coupled with collateral cleavage of bystander RNAs that is often observed in previous articles.[20,23,24]

One distinctive characteristic of Cas13 systems is their collateral activity. When Cas13 recognizes viral RNAs with specificity, it triggers the nonspecific RNase function of Cas13, causing the degradation of both intended target RNAs and unintended nontarget RNAs. Mechanically, the binding of target RNA prompts a change in the conformation of Cas13, leading to the activation of an endoribonuclease activity on the surface of Cas13. As a result, both the target RNA and nearby bystander RNAs are cleaved.[25] Although this collateral cleavage may limit the potential of Cas13 for therapeutic applications, we hypothesized that it could be leveraged in mosquitoes to combat viral infections, providing a basis for the development of flexible antiviral technologies.

This high on-target activity could be leveraged in mosquitoes to combat viral infections, providing a basis for the development of flexible antiviral technologies. The transmission of CHIKV by *Aedes* mosquitoes is dependent on the viral titer, with higher titers leading to increased mosquito infections.[26–30] Therefore, the most effective approaches to stop transmission is to eliminate mosquitoes carrying infectious CHIKV. To identify tools capable of eradicating mosquitoes after CHIKV infection, in this study we exploit the properties of Cas13 for programmable viral RNA targeting in mosquitoes.

To develop this innovation, we use the *Ruminococcus flavefaciens* RfxCas13d ribonuclease (herein referred to as CasRx),[17] which possesses robust RNA cleavage activity. We genetically encoded CasRx expression in mosquitoes and demonstrated its efficacy by targeting two nonessential genes. Subsequently, we biochemically screen the activity of guide RNA (gRNAs) targeting CHIKV using a sensitive enzymatic nucleic acid sequence reporter (SENSR).[31]

In this way, we selected gRNA with high on-target and high collateral activity *in vitro* (collateral cleavage speed <10 min per each gRNA) by using the SENSR system and we then use these effective gRNAs to engineer an antiviral sensor in *Aedes aegypti* termed vRNA Expression Activates Poisonous Effector Ribonuclease (REAPER). Akin to a Trojan horse resting in wait to eliminate its enemy, REAPER remains inactive in the absence of its target viral RNA and becomes activated upon viral infection. We demonstrate that REAPER is programmed to directly target deadly arboviruses such as CHIKV, resulting in reduced viral transmission and even mortality of infected mosquitoes.

Materials and Methods

Mosquito rearing and maintenance

All *Ae. aegypti* lines used in this study were generated from the Liverpool strain. Colonies were reared at 27°C ± 1°C with 70–80% relative humidity and a 12-h light/dark cycle. Adults were fed 0.3 M aqueous sucrose *ad libitum.* To collect eggs, mature females were blood-fed on anesthetized mice. Oviposition cups were provided 3 days post-blood-meal, and the eggs were collected and aged for 3 days before hatching. Mature eggs were submerged in deionized H_2O and placed overnight in a vacuum chamber set to 677 Millibar Pressure Unit (mbar). Emerged larvae were reared in plastic containers (Sterilite) with ~3 L of deionized H_2O and fed daily with fish food (Tetramin).

Design and cloning of constructs

Gibson enzymatic assembly was used to construct all cloned plasmids. To generate the CasRx expressing construct OA-1050T (Addgene plasmid #191374), the plasmid OA-1050E (Addgene plasmid #132416) was used as a backbone. A DNA fragment containing the *Ae. aegypti* ubiquitin promoter was amplified from the Addgene plasmid #100580 using primers 874F/1050T.C1 and was inserted using the *Avr*II and *Pac*I restriction enzyme sites.

To generate the *Ae. aegypti* codon-optimized CasRx expressing construct OA-1163A (Addgene plasmid #194001), the OA-1050T plasmid was cut by restriction enzymes *Pac*I and NheI to remove CasRx. The codon-optimized CasRx fragment was synthesized from GenScript (GenScript USA, Inc., Piscataway, NJ, USA) and then cloned in.

In addition, we designed three gRNA-array constructs, OA-1085F (Addgene plasmid #191375), OA-1085L (Addgene plasmid #191376), and OA-1093B (Addgene plasmid #194003), targeting *yellow*, enhanced green fluorescent protein (EGFP), and CHIKV, respectively. We synthesized OA-1085F and OA-1093B using Gene Synthesis (GenScript USA, Inc.), with each plasmid containing *piggyBac*, 3xp3-tdTomato, the U6b (AAEL017774) promoter, and 3′UTR in addition to an array of four programmed transcript-targeting spacers each positioned between the CasRx-specific direct repeats (36 nt in length) with a conserved 5′-AAAAC motif at the 3′ end of the direct repeat followed by a 7-thymine terminator.[17]

This CRISPR array is then transcribed into pre-crRNA and processed into mature crRNA by the CasRx enzyme. Finally, the crRNA guides the CasRx protein to target CHIKV RNA for degradation. To generate construct OA-1085L, a plasmid (Addgene #120363) containing *piggyBac* and 3xp3-tdTomato was used as the backbone, which was linearized at the restriction enzyme sites *Avr*II and *Asc*I to clone in the designed fragment. This insert fragment was synthesized using Gene Synthesis (GenScript USA, Inc.) to contain the U6b (AAEL017774) promoter and 3′UTR in addition to the crRNA array containing the four spacers, a 7-thymine terminator, and then the Opie2-EGFP marker.

All primer sequences can be found in Supplementary Table S21. All plasmids and annotated DNA sequence maps are available at www.addgene.com under accession numbers 191374 (OA-1050T), 191375 (OA-1085F), 191376 (OA-1085L), 194001 (OA-1163A), and 194003 (OA-1093B).

Generation of transgenic lines

Transgenic lines were generated by microinjecting preblastoderm embryos (0.5–1 h old) with a mixture of the piggyBac plasmid (200 ng/μL) and a transposase helper plasmid (phsp-Pbac; 200 ng/μL). Embryonic collection and microinjections were performed following previously established procedures.[32,33] Four days post-microinjection, G_0 embryos were hatched in deionized H_2O under vacuum (20 inHg). Surviving G_0 pupae were sex-separated into ♀ or ♂ cages (5 G_0s per cage). WT pupae of the opposite sex and of a similar age were added to cages at a 5:1 ratio (WT:G_0). Several days post-eclosion ($\sim$4–7), a blood meal was provided, and the eggs were collected, aged, and hatched.

Hatched G_1 larvae were screened and sorted for the expression of relevant fluorescent markers using a fluorescent stereo microscope (Leica M165FC). To isolate separate insertion events, selected transformants were individually backcrossed to WT (5:1 ratios of WT:G_0), and separate lines were established. Each individual line was maintained as mixtures of homozygotes and heterozygotes with the periodic selective elimination of WTs. In total, 5 Ub:CasRx-NLS, 3 U6b:gRNA^{yellow}, 1 U6b:gRNA^{EGFP}, 10 Ub:CasRx-NES, and 1 gRNA lines targeting CHIKV were created (Supplementary Table S2).

Generating and screening for CasRx/gRNA transheterozygote

To genetically assess the efficiency of CasRx ribonuclease activity, we bidirectionally crossed the highest Ub:CasRx expressing lines to gRNA-expressing lines targeting either the *yellow* (Ub6:gRNA$^{yellow\text{-}A}$, Ub6:gRNA$^{yellow\text{-}B}$, Ub6:gRNA$^{yellow\text{-}C}$) or EGFP (Ub6:gRNA^{EGFP}) transcripts. After allowing the crosses to mate for 3 days, females were blood-fed for 2 consecutive days. Three days after blood-feeding, females were individually captured in plastic vials lined with moistened paper. Captured females were kept for 2 days to allow for egg laying and were removed afterward.

Collected eggs were either processed for RNA collection or hatched to screen progeny. The number of eggs on the moistened paper and larvae were then recorded and used to calculate the hatching rate. The larvae were also screened for the number of transheterozygotes, which was used to calculate the inheritance and penetrance of the observable phenotypes. Mosquito larvae and pupae were imaged using different filters (ET-EGFP, CF/YF/mC, mCherry, and white) on a Leica M165FC fluorescent stereomicroscope equipped with a Leica DMC4500 color camera.

The hatching rate was calculated as the ratio of number of larvae to the number of eggs, and the penetrance of the EGFP-targeting phenotype was calculated as the ratio between the number of transheterozygotes showing EGFP reduction and the total number of transheterozygotes. Statistical analyses were performed using the one-way analysis of variance (ANOVA) and Tukey's multiple-comparison tests in RStudio (version 1.2.5033, © 2009-2019).

Total RNA collection and quantitative PCR

To directly select the lines with the highest CasRx expression, 10 adult individuals were collected from each of the 5 selected Ub:CasRx-NLS lines and from each of the 10 selected Ub:*Ae*CasRx-NES lines listed in Supplementary Table S2. In addition, to directly observe and quantify the reduction in targeted *yellow* and EGFP transcripts by the Ub:CasRx-NLS or Ub:*Ae*CasRx-NES lines, we collected transheterozygous embryos and transheterozygous larvae for RNA extraction and subsequent quantitative PCR (qPCR) and RNA sequencing.

Embryos were collected 24 h post-oviposition from the F1 transheterozygous line (Ub:CasRx-NLS/U6b-gRNA$^{yellow\text{-}A}$) as well as the parental lines (Ub:CasRx-NLS; U6b-gRNA$^{yellow\text{-}A}$). Three biological replicates were collected per line for a total of 15 samples.

In addition, to quantify the knockdown of *yellow* and EGFP in surviving larvae, third instar larvae were used for RNA extraction and subsequent qPCR analysis and RNA sequencing. For this, another 3 biological replicates were collected per line for a total of 18 samples, including 3 transheterozygous lines (1 targeting yellow and 2 targeting EGFP at different visual levels) and the 3 parental controls. Embryos and larvae were also collected for qPCR analysis of Ub:*Ae*CasRx-NES crosses with gRNA lines targeting *yellow* and EGFP. Total RNA was extracted using a Qiagen RNeasy Mini Kit (74104; Qiagen).

After extraction, the total RNA was treated with an Invitrogen DNase treatment kit (AM1906; Invitrogen). RNA concentration was analyzed using a Nanodrop OneC UV-vis spectrophotometer (ThermoFisher NDONEC- W). About 1 μg of total RNA was used to synthesize cDNA with a RevertAid H Minus First Strand cDNA Synthesis kit (*Thermo Fisher Scientific*). cDNA was diluted 50 times before use in real-time quantitative PCR (RT-qPCR). RT-qPCR was performed with SYBR green (qPCRBIO SyGreen Blue Mix Separate-ROX; Cat No. 17-507B; Genesee Scientific), using 4 μL of diluted cDNA for each 20 μL reaction containing a final primer concentration of 200 nM and 10 μL of SYBR green buffer solution.

Three technical replicates were performed for each reaction to correct for pipetting errors. The following qPCR profile was used on the LightCycler® instrument (Roche): 3 min of activation phase at 95°C, 40 cycles of 5 s at 95°C, and 30 s at 60°C. Primers are listed in Supplementary Table S21. The *rpl32* gene was used as a Ref.[34] to calculate relative expression levels of *yellow* and EGFP using the manufacturer's software and the delta-delta Ct method ($2^{-\Delta\Delta Ct}$). Differences in the expression of *yellow* and EGFP between the controls and transheterozygous lines were statistically tested using the one-way ANOVA and Tukey's multiple-comparison test in RStudio (version 1.2.5033).

The RNA samples collected for crosses between the Ub:CasRx-NLS and gRNA lines with relative controls were also used to perform RNA-seq analyses to further validate the qPCR analysis as well as detect the collateral activity of CasRx resulting in misregulation of the whole transcriptome. For these analyses, mRNA was isolated from ~1 μg of total RNA using NEBNext Poly(A) mRNA Magnetic Isolation Module (#E7490; NEB). RNA integrity was assessed using the RNA 6000 Pico Kit for Bioanalyzer (5067-1513; Agilent Technologies), and RNA-seq libraries were constructed using NEBNext Ultra II RNA Library Prep Kit for Illumina (#E7770; NEB) following manufacturer's instructions.

Libraries were quantified using a Qubit dsDNA HS Kit (#Q32854; ThermoFisher Scientific), and the size distribution was confirmed using a High Sensitivity DNA Kit for Bioanalyzer (#5067-4626; Agilent Technologies). Libraries were sequenced on an Illumina HiSeq2500 in single read mode with a read length of 50 nt and sequencing depth of 20 million reads per library. Basecalling was performed with RTA 1.18.64 followed by conversion to FASTQ with bcl2fastq 1.8.4.

Quantification and differential expression analysis

For these studies, the RNA was treated and sequenced as aforementioned. The reads were mapped to *Ae. aegypti* genome AaegL5.0 (GCF_002204515.2) supplemented with the PUb-dCas9 transgene sequence using STAR.[35] Gene expression was then quantified using featureCounts against the NCBI *Ae. aegypti* Annotation Release 101 (GCF_002204515.2_AaegL5.0_genomic.gtf). TPM values were calculated from counts produced by featureCounts and were combined (Supplementary Tables S4 and S6). Hierarchical clustering and PCA analyses were performed in R and were plotted using R package ggplot2.

Differential expression analyses between the controls (Ub:CasRx-NLS; U6b-gRNA$^{yellow\text{-}A}$ and U6b-gRNA^{EGFP}) and transheterozygous lines (Ub:CasRx-NLS/U6b-gRNA$^{yellow\text{-}A}$ and Ub:CasRx-NLS/U6b-gRNA^{EGFP}) were performed with DESeq2 (Supplementary Tables S7, S8, S11, S12, S14, S15, and S16). The Illumina RNA sequencing data have been deposited to the NCBI Sequence Read Archive (SRA), accession number #PRJNA912231 (reviewer link: https://dataview.ncbi.nlm.nih.gov/object/PRJNA912231?reviewer=7ll0k7o7hauq2eh8kbv16mjbj9).

Phenotypic screening

To collect eggs laid from single-pair mating events, female and male mosquitoes were allowed to mate for 3 days post-eclosion. Females were given a blood meal for 2 consecutive days. The following day, blood-fed females were independently placed into separate plastic drosophila vials lined with wet paper and plugged with a foam plug. The females were kept in the vials for 2–3 days for egg laying. After oviposition onto the paper, females were released into a small cage, and the laid eggs were collected, counted, and allowed to mature to full development (~4 days) in their original vials.

Mature eggs were hatched in their original vial under vacuum overnight. After hatching, the egg papers were removed from the vials to provide more space for larval growth.

At the L3 stage, the progeny were screened, scored, and counted for the expression of opie2-dsRed, 3xP3-tdTomato, and opie2-EGFP using a fluorescence-equipped stereoscope (Leica M165FC). The difference in numbers between the total larval counts compared with the total egg counts were considered to have died during embryonic or early larval stages. Surviving transheterozygous individuals were collected for further observation and analysis. Mosquito larvae and pupae were also imaged using a Leica DMC4500 color camera.

The hatching rate was calculated as the ratio of the number of larvae to the number of eggs, and the penetrance of the EGFP-targeting phenotype was calculated as the ratio between the number of transheterozygotes showing visual EGFP reduction to the total number of transheterozygotes. Statistical analyses were performed using the one-way ANOVA and Tukey's multiple-comparison test in RStudio (version 1.2.5033, © 2009–2019).

Design and selection of the viral target sites

For CHIKV gRNA arrays, CHIKV genomes (469) were downloaded from Virus Pathogen Database and Analysis Resource (ViPR, www.viprbrc.org) and aligned with the CHIKV LR2006_OPY1 strain (GenBank DQ443544) MUSCLE in MegAlign Pro 17 (Supplementary Material). Aligned strains were found to have >90% identity to CHIKV LR2006_OPY1. Alignment of the laboratory strain used (isolate 06113879, Mauritius strain, GenBank MH229986) found 99.64% identity between both strains.

Consensus sequences from alignments were then used to identify conserved regions of interest of at least 30 nt in length in the nsp coding regions of CHIKV. Two suitable target sequences were found in nsp1, nsp2 regions, and two within the nsp4 coding region (Supplementary Fig. S5). We then generated four gRNAs, one gRNA for each of the identified conserved regions (Supplementary Table S20).

SENSR assays

SENSR assays were performed as described previously[31] using a two-step nucleic acid detection protocol. In brief, target sequences were first amplified in a 30 min isothermal preamplification reaction by combining reverse transcription with recombinase polymerase amplification (RT-RPA). RT-RPA primers were designed to amplify 30 bp gRNA spacer complement regions flanked by 30 bp priming regions from the synthetic vRNA template while simultaneously incorporating a T7 promoter sequence and ''GGG'' into the 5′ end of the dsDNA gene fragment to increase transcription efficiency.[36]

The RT-RPA primer sequences and synthetic target sequences can be found in Supplementary Table S21. The RT-RPA was performed at 42°C for 30 min by combining M-MuLV-RT (#M0253L; NEB) with TwistAmp Basic (#TABAS03KIT; TwistDx). The final conditions for the optimized (28.5% sample input) RT-RPA protocol in a 10-μL reaction are as follows: 5.9 μL rehydration buffer (TwistDx), 0.35 μL primer mix (10 μM each), 0.4 μL reverse transcriptase (200 U/μL), 0.5 μL MgOAc (280 mM), and 2.85 μL vRNA.

The RT-RPA reaction was then transferred to a second reaction, termed the Cas cleavage reaction (CCR), which contained a T7 polymerase and the CasRx ribonucleoprotein. In the second reaction, *in vitro* transcription was coupled with the cleavage assay and a fluorescence readout using 6-carboxyfluorescein (6-FAM). A previously validated[31] 6-nt poly-U probe (FRU) conjugated to a 5′ 6-FAM and a 3′ IABlkFQ (Iowa Black Fluorescence Quencher) was designed and custom-ordered from IDT.

Detection experiments were performed in 20-μL reactions by adding the following reagents to the 10-μL RT-RPA preamplification reaction: 2.82 μL water, 0.4 μL 4-(2-hydroxyethyl)-1-piperazineethanesulfonic acid pH 7.2 (1 M), 0.18 μL $MgCl_2$ (1 M), 1 μL rNTPs (25 mM each), 2 μL CasRx (55.4 ng/μL), 1 μL RNase inhibitor (40 U/μL), 0.6 μL T7 Polymerase (50 U/μL), 1 μL gRNA (10 ng/μL), and 1 μL FRU probe (2 μM). Experiments were immediately run on a LightCycler 96 (#05815916001; Roche) at 37°C for 60 min with the following acquisition protocol: 5 s acquisition followed by 5 s incubation for the first 15 min, followed by 5 s acquisition and 55 s incubation for up to 45 min.

Fluorescence readouts were analyzed by calculating the background-subtracted fluorescence of each timepoint and by subtracting the initial fluorescence value from the final value. Statistical significance was calculated using a one-way ANOVA followed by specified multiple comparison tests ($n = 3$). The collateral cleavage speed of each gRNA was calculated from the half-maximum fluorescence (see Ref.[31]).

Vector competence assay

All experiments were performed under biosafety level 3 conditions in the insectary at the Australian Centre for Disease Preparedness as previously described.[10,37] The CHIKV (isolate 06113879, Mauritius strain, GenBank MH229986) viral strains grown in Vero cells were used for viral challenge experiments in mosquitoes. In brief, female mosquitoes were challenged with an infected

blood meal ($\sim 1 \times 10^6$ median tissue culture infective dose [$TCID_{50}$]/mL) through membrane feeding using chicken blood and skin.

For determining viral dissemination and infection frequency, whole mosquitoes were collected at 14 days post-challenge, with all deceased mosquitoes collected daily. Daily observations were performed to track mosquito survival during the course of the experiment. The Mantel–Cox statistical test for survival was performed using GraphPad Prism (Version 9.5.0).

Total RNA extraction and real-time quantitative reverse transcription PCR (qRT-PCR) of viral gene expression

Total RNA was extracted from homogenized whole mosquitoes using the Qiagen RNeasy plus mini kit (74136; Qiagen). After extraction, cDNA synthesis was performed with $\sim 1\,\mu$g of RNA using the Superscript III First-Strand synthesis system (18080051; *Thermo Fisher Scientific*). qRT-PCR was performed with TB Green Premix Ex Taq II (RR820L; Takara). Each 20 μL reaction contained 2 μL of cDNA and 10 μL of TB Green solution with a final primer concentration of 200 nM. Three technical replicates were performed for each reaction to correct for pipetting errors.

The following qPCR profile was used on the QuantStudio 6 Real-Time PCR system (*Thermo Fisher Scientific*): 30 s at 95°C (hold stage), 40 cycles of 5 s at 95°C, and 30 s at 60°C followed by a melt curve stage of 15 s at 95°C, 60 s at 60°C, and 15 s at 95°C. The ribosomal protein S17 (*rps17*) gene[34] was used as a reference to calculate the expression of CHIKV E1 using the delta-delta Ct method ($2^{-\Delta\Delta Ct}$). Standard curves were created for both targets (Supplementary Fig. S8). Mann-Whitney *U* test statistical analysis was performed on all samples using GraphPad Prism (Version 9.5.0).

Creating standard curve with plasmid template for qPCR quantification.

To create a standard curve, plasmids were individually synthesized (Integrated DNA technologies) with cloned target sequences of either Chikungunya E1 or *Ae. aegypti rps17* Serial dilutions were assessed through qPCR (as described previously) to create a standard curve. These curves were then used to determine concentration of our targets in all experiments.

Results

Generation of a programmable RNA-targeting platform in *Ae. aegypti*

To generate a platform for programmable RNA targeting, we created 15 transgenic *Ae. aegypti* lines that genetically encoded CasRx. CasRx expression was driven by a broadly expressed ubiquitin L40 (Ub) promoter[38] with either a codon optimized nuclear localization signal (NLS) or a codon-optimized CasRx fused with a nuclear export signal (NES) (Supplementary Fig. S1). CasRx expression levels were assessed through RNA sequencing and qPCR.

Lines with the highest expression levels (Supplementary Tables S1 and S2) were genetically crossed with two transgenic lines expressing gRNA arrays engineered to target either an endogenous *Ae. aegypti yellow* transcript or the reporter EGFP transcript, allowing for visual quantification of expression levels. The expression of these gRNA arrays was driven by a U6 noncoding small nuclear RNA polymerase III promoter ($U6b{:}gRNA_{array}$)[39] (Supplementary Fig. S1).

The resulting progeny were assessed for hatching rates, visual phenotypes, zygosity, and misexpression of the target/nontarget genes quantified using both qPCR and RNA sequencing (Figs. 1 and 2; Supplementary Figs. S2–S4).

Targeting *yellow* resulted in high embryonic lethality (Supplementary Table S3) with only 60% of the crosses producing viable transheterozygous eggs (Ub:CasRx/+; $U6b{:}gRNA^{yellow}$/+) (Fig. 1B; Supplementary Fig. S3A). Remarkably, only 7.59% of transheterozygotes survived to adulthood, despite *yellow* being dispensable for survival.[40] Both qPCR and RNA sequencing detected a remarkable 13-fold reduction in *yellow* transcripts in the transheterozygote embryos as compared with controls, confirming programmed on-target disruption (Fig. 1C; Supplementary Fig. S2A).

Targeting EGFP also resulted in lethality and a reduced hatching rate of $\sim$43% (Fig. 1D). The surviving transheterozygotes were evaluated by visually quantifying EGFP fluorescence (Fig. 1F, G), which was reduced by an average of 70.27% (Fig. 1D; Supplementary Table S5). In addition, the phenotypic data are in agreement with both qPCR and RNAseq analysis that revealed a significant 2.11- to 4.36-fold reduction of EGFP in larval samples (Fig. 1E; Supplementary Fig. S2B and Supplementary Table S6).

Although visible GFP protein reduction was difficult to score in some surviving larvae, GFP mRNA reduction was confirmed by qPCR and RNA sequencing (Fig. 1E). Collectively, these results offer convincing proof of CasRx's capacity to selectively decrease the expression of desired genes. However, the observed elevated mortality rates indicate potential toxicity concerns.

To estimate the degree of CasRx toxicity, we performed differential expression using transcriptome wide RNA sequencing (Fig. 2; Supplementary Tables S6–S17). Comparing transheterozygotes targeting *yellow* at the embryonic stage to the controls showed that remarkably

~45% of the transcriptome was misexpressed, either under- or overexpressed (false discovery rate [FDR] <0.05) (Fig. 2A, C; Supplementary Tables S11 and S12).

The main category of misexpressed genes consisted of genes involved in structural components of the cuticle (fold change > −10; FDR <0.05), which perhaps is indicative of collateral activity largely occurring in cells that express *yellow*, as this is an important factor in cuticle pigmentation (Fig. 2C; Supplementary Table S13). In surviving transheterozygotes, only 24% of the genes were misexpressed, although these also had much lower fold changes (Fig. 2B, C; Supplementary Table S14).

Comparing the differential expression between transheterozygotes targeting EGFP and the controls showed that ~10% of the transcriptome was misexpressed. Half of these misexpressed genes, representing ~5% of the transcriptome, were downregulated genes (Fig. 2D–F; Supplementary Tables S15–S17). Similar results were also observed when using CasRx fused with an NES (Supplementary Fig. S4; Supplementary Tables S18 and S19), indicating that the presence of NLS or NES does not affect CasRx activity.

These data confirm the programmable knockdown of targeted genes, although with a significant impact on the transcriptome.

Generation of REAPER in *Ae. aegypti*

The high on-target activity of CasRx is coupled with collateral cleavage of bystander RNAs that has been a feature previously observed for CasRx.[20,23,24] To exploit the collateral activity of CasRx, gRNAs targeting CHIKV were synthesized and screened for their *in vitro* collateral cleavage efficiency. Four CHIKV coding regions of the nonstructural protein (nsp) were targeted by designing two gRNA targeting nsp1 and nsp2 regions, and two targeting the nsp4 coding region for screening[41] (Supplementary Table S20;Supplementary Fig. S5).

To determine which gRNA resulted in the highest level of collateral activity, we used SENSR[31] in which the gRNAs were independently challenged against synthetic ssRNA templates mimicking the respective virus. In this study, the presence of the viral template triggers the activation of CasRx/gRNA complex activity *in vitro*, and a fluorescent readout indicates the effectiveness of the deployed gRNAs for inducing collateral activity. Upon activation, the CasRx collateral activity cleaves a quenched probe to produce a fluorescent signal (Fig. 3A, B).

All CHIKV gRNAs resulted in rapid collateral activity (Fig. 3C). Importantly, the data indicate that in the absence of the target RNA, the collateral activity is null, confirming that the presence of a target sequence is necessary to activate CasRx activity[31] (Fig. 3B, D). We noticed in this study that a high level of synthetic target seemed to trigger greater collateral activity. To confirm this observation and identify how target concentration influences collateral activity, we next performed a serial dilution of the synthetic templates in the SENSR assay. The results demonstrated a direct relationship between target concentration and collateral activity (Fig. 3D, E), confirming that high target levels trigger high collateral activity.

With these results in hand, we next engineered a transgenic line expressing the four gRNAs tested with SENSR (U6b:gRNA^{CHIKV}) and crossed it to the CasRx lines, encoding either an NLS (Ub:CasRx-NLS) or NES (Ub:CasRx-NES-A and Ub:CasRx-NES-B). To activate the REAPER system, transheterozygous mosquitoes were challenged with a CHIKV infection and the analysis of viral reduction and/or mosquito viability at 14 days postinfection was recorded to test the efficiency of these lines (Fig. 4A).

As control, survival of transheterozygous mosquitoes was also recorded for 14 days after a noninfected blood meal (Supplementary Fig. S7). In the presence of Ub:CasRx-NLS, the mosquitos, challenged by a CHIKV infection, showed a minimal effect on the viral genome copy numbers, infection rates, and survival as compared with the controls (Supplementary Fig. S6). In contrast, the U6b:gRNA^{CHIKV} mosquito line crossed with either Ub:CasRx-NES-A or Ub:CasRx-NES-B showed significant decreases in both survival, as about 35% of the mosquitoes died within 5 days post-CHIKV infection (Fig. 4B), and viral titers indicating that the NES is effective at targeting viruses such as CHIKV that replicate in the cytoplasm (Fig. 4C).

On the contrary, noninfected transheterozygotes mosquitoes (Ub:CasRx-NES-A or Ub:CasRx-NES-B crossed with U6b:gRNA^{CHIKV}) showed no differences in survival compared with controls (Supplementary Fig. S7). Taken together these data indicate that REAPER is an effective strategy to target vRNA and even kill infected mosquitoes.

Discussion

In this study, we addressed the need for engineering programmable and effective methods for controlling viral transmission through mosquito vectors by generating a Cas13-based antiviral system termed REAPER in *Ae. aegypti*. REAPER exploits the activity of CasRx to impede viral replication and/or kill infected mosquitos, limiting viral transmission. Importantly, in true Trojan horse manner, REAPER lies in wait for the presence of its ''enemy'' and is only activated after viral infection. With our system, we demonstrate reduction of CHIKV replication in *Ae. aegypti*.

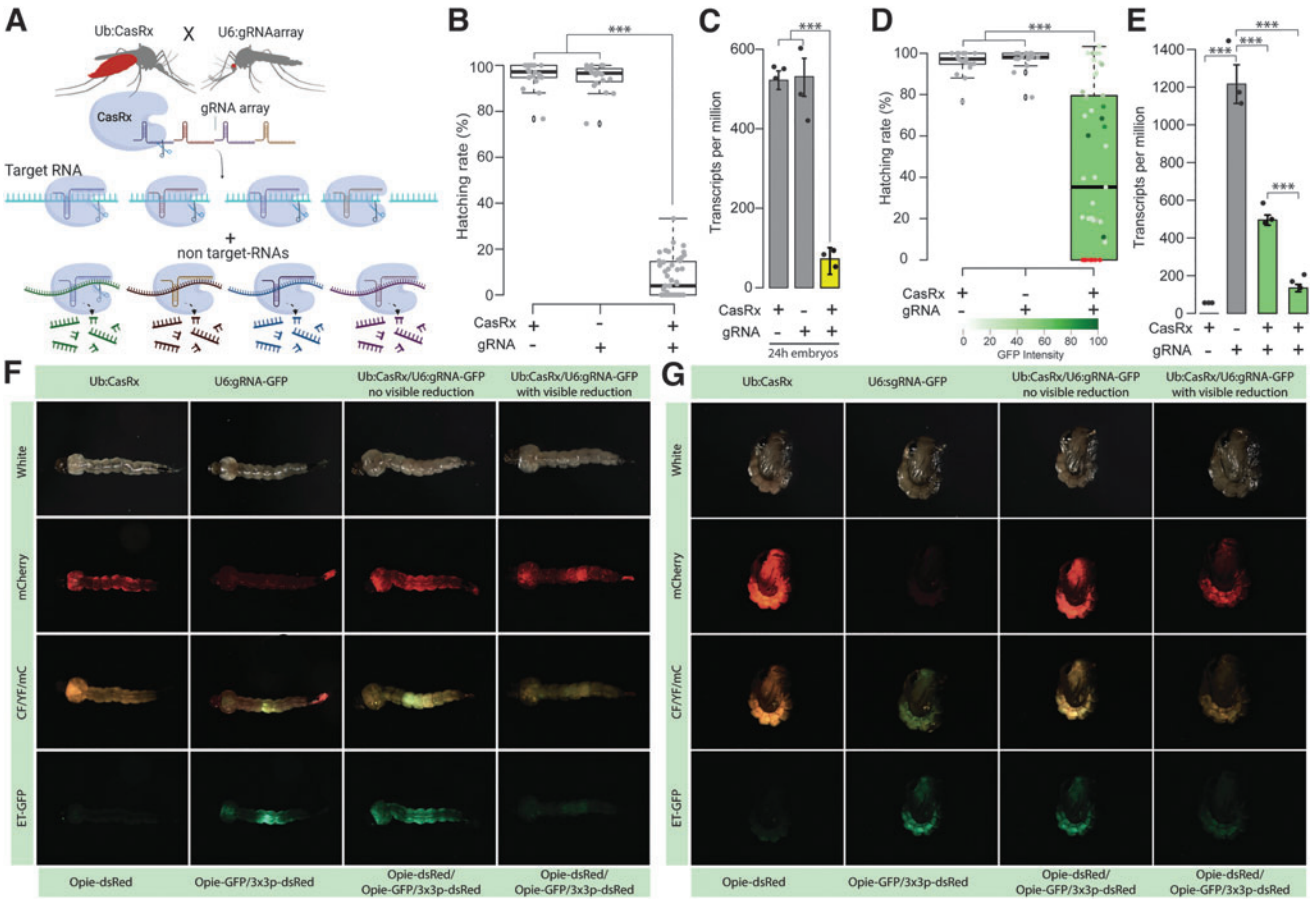

FIG. 1. Assessment of transcript reduction mediated by CasRx. **(A)** Schematic representation of the binary system used for the proof-of-concept studies evaluating the candidate target genes. The lines are composed of CasRx and a gRNA array targeting the gene of interest inducing collateral cleavage of bystander RNAs. **(B)** Hatching rate of parental lines and transheterozygotes targeting yellow. Asterisks indicate significant differences by one-way ANOVA with Tukey's multiple-comparison test (***$p < 0.001$), $n = 20$–50. **(C)** Relative expression measured by qPCR in control and transheterozygotes embryos. Asterisks indicate significant differences by one-way ANOVA with Tukey's multiple-comparison test (***$p < 0.001$), bars represent standard errors, $n = 3$ biological replicates with 5 mosquitoes each. **(D)** Hatching rate of parental lines and transheterozygotes targeting EGFP. Phenotype penetrance is depicted by green shading in the box plot, with colors ranging from light green (low EGFP levels) to dark green (high EGFP levels). Red dots represent dead individuals and thus nonquantifiable EGFP. Asterisks indicate a significant reduction in the hatching rate in transheterozygotes by one-way ANOVA with Tukey's multiple-comparison test (***$p < 0.001$), $n = 20$–50. **(E)** Relative expression measured by qPCR in control and transheterozygote larvae in EGFP. The two transheterozygote groups represent larvae with no visible reduction in EGFP and with visible reduction of EGFP, respectively. Asterisks indicate significant differences by one-way ANOVA with Tukey's multiple-comparison test (***$p < 0.001$), bars represent standard errors, $n = 3$ biological replicates with 5 mosquitoes each. **(F, G)** EGFP reduction at larval and pupal stages, respectively. mCherry represents the red fluorescent filter, ET-EGFP represents the green fluorescent filter, and CF/YF/mC represents the triple hybrid filter for detecting blue, yellow, and red fluorescence. ANOVA, analysis of variance; CF/YF/mC; EGFP; ET-EGFP; qPCR, quantitative PCR; YF.

The foundation of the REAPER technology lies in its efficient RNA-targeting mechanism. To create an effective strategy, we designed and selected viral target sites through bioinformatic analysis. We also further confirmed substantial collateral activity *in vitro* using the previously established SENSR system. We observed rapid and robust responses for all tested gRNAs.

Since there is a need for a technology that can detect multiple virus serotypes or different viruses, we used *in vitro* data information to develop a multiplexed

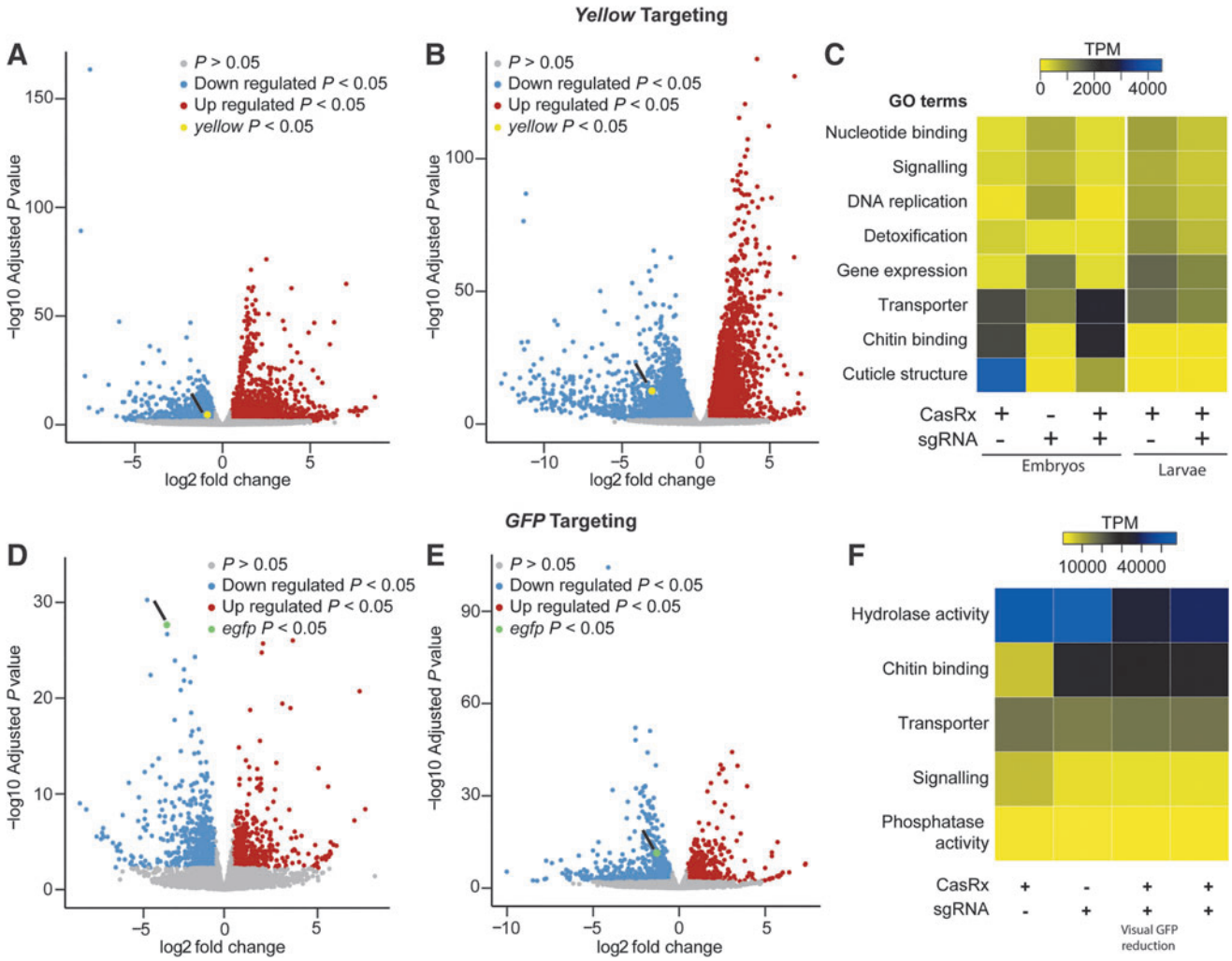

FIG. 2. Transcriptome differential expression analysis. **(A)** RNAseq results in 24-h-old eggs and **(B)** in third instar larvae comparing transheterozygotes targeting yellow to the CasRx expressing control line. Blue dots represent downregulated genes with $p < 0.05$, and red dots represent overexpressed genes with $p < 0.05$. **(C)** Heat map of gene functions with the twofold difference in expression level among different treatments and FDR <0.05 when targeting the yellow gene. Expression levels are represented by colors ranging from yellow (lowest expression) to blue (highest expression). Cuticle and chitin binding are the main genes being downregulated in the presence of both CasRx and crRNA. **(D)** RNAseq results in third instar larvae with a visible EGFP reduction and **(E)** in the third instar larvae that do not show visible EGFP reduction comparing transheterozygotes targeting *GFP* to CasRx expressing control line. Blue dots represent downregulated genes with $p < 0.05$ and red dots represent overexpressed genes with $p < 0.05$. **(F)** Heat map of gene functions with the twofold difference in expression level among different treatments and FDR <0.05 when targeting EGFP transgene. Expression levels are represented by colors ranging from yellow (lowest expression) to blue (highest expression). Only small differences in chitin binding and signaling genes are detected. FDR, false discovery rate; GFP, green fluorescent protein.

strategy to target four target regions of CHIKV. Although all gRNAs tested showed this rapid and robust collateral activity, we observed differences in speed and intensity. Nevertheless all CHIKV gRNAs were able to induce lethality *in vivo*. Previous study has described differences in interference efficiencies from different gRNAs,[42,43] suggesting that target RNA accessibility might impact CasRx activity.

However, there are limited comprehensive studies of collateral activity, although a greater understanding

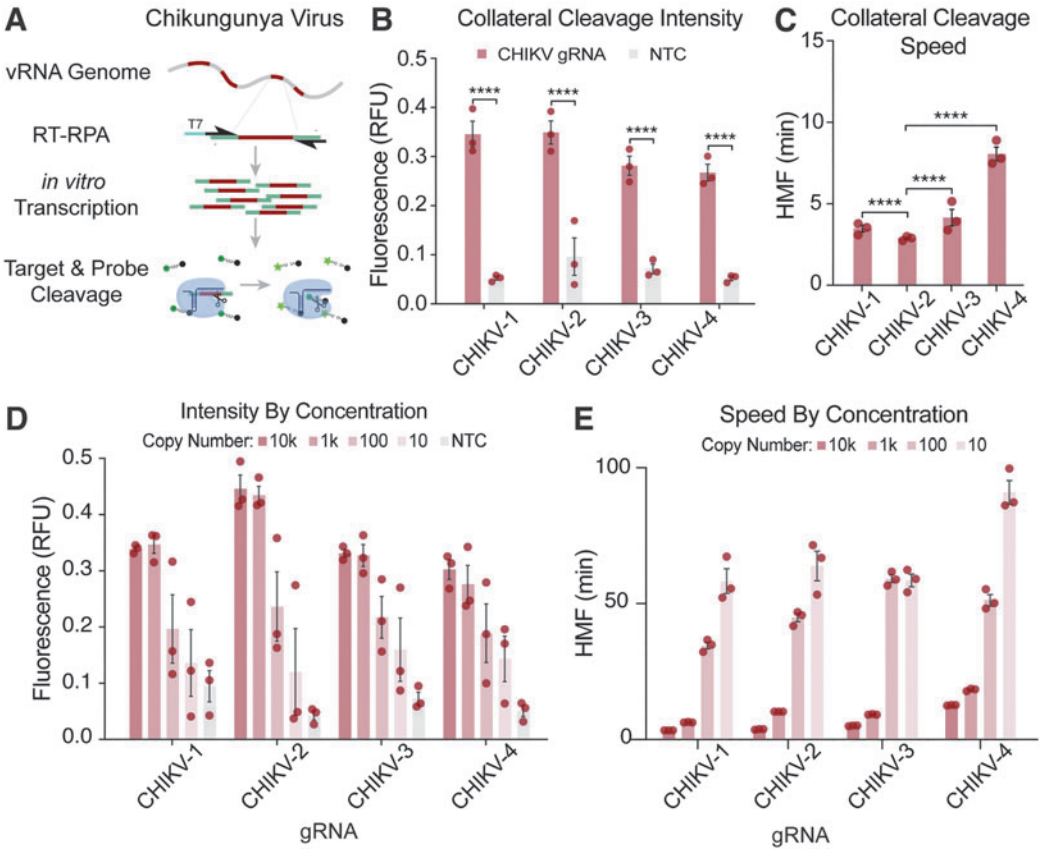

FIG. 3. Analysis of gRNA-dependent collateral activity targeting CHIKV. **(A)** Schematic representation of the SENSR system used to determine the collateral cleavage activity of selected gRNAs. The detection protocol requires that the specific target sequences within the viral RNA are RT into cDNA and amplified by RPA at 42°C for 30 min. During amplification, a T7 promoter is incorporated into the 5′ terminus of the amplicons (T7, blue). In the next step, both *in vitro* transcription and CasRx collateral cleavage occur simultaneously. Finally, the recognition and cleavage of the target RNA sequence complementary to the gRNA induce collateral cleavage of bystander RNA molecules. Collateral cleavage of a modified probe conjugated to 6-FAM, and a fluorescence quencher facilitates readout by fluorescence. **(B)** Initial characterization of the collateral activity for each gRNA targeting CHIKV. SENSR analysis was performed against 10,000 copies/μL of the synthetic target. The fluorescence signal represents the background-subtracted signal. Statistical significance was calculated using Sidak's multiple comparisons test (****$p < 0.0001$, $n = 3$), bars represent standard errors. **(C)** Collateral cleavage speed of each gRNA calculated using HMF analysis (see Materials and Methods section), where a lower HMF indicates faster collateral activity. Statistical significance was calculated using Tukey's multiple comparison test (****$p < 0.0001$, $n = 3$), bars represent standard errors. **(D)** Intensity of signal from SENSR assay for each gRNA along a concentration gradient. The fluorescence signal represents the background-subtracted signal ($n = 3$), bars represent standard errors. **(E)** Speed of cleavage along concentration gradient for each gRNA used to target CHIKV. The speed of collateral activity is represented using an HMF analysis ($n = 3$), bars represent standard errors. 6-FAM, 6-carboxyfluorescein; CHIKV, chikungunya; gRNA, guide RNA; HMF, half-maximum fluorescence; RPA, recombinase polymerase amplification; RT, reverse transcribed; SENSR, sensitive enzymatic nucleic acid sequence reporter.

of this phenomenon could improve Cas-based Trojan horse systems and other applications that exploit collateral activity. SENSR data confirmed that the presence of a target sequence is necessary to activate CasRx collateral activity enabling us to develop a system that is dormant in uninfected mosquitoes and activated after infection.

The system reduced viral replication and, therefore, transmission by mosquitoes by either knocking down viral RNA expression or killing the infected mosquitoes.

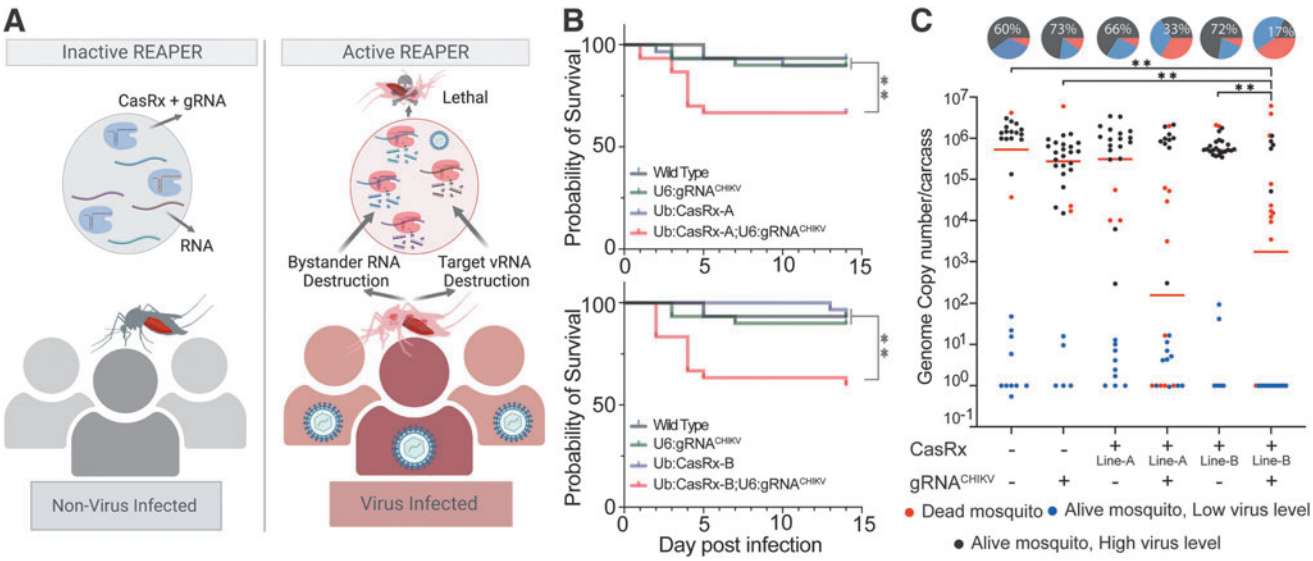

FIG. 4. Viral challenge assays. **(A)** Schematics representation of the REAPER system. REAPER remains inactive in uninfected mosquitoes and is activated in the presence of the targeted virus. Once activated, REAPER induces degradation of viral RNA with additional collateral cleavage of bystander RNAs, leading to lethality. **(B)** Adult survival curves (log-rank Mantel–Cox test) of virus exposed females per treatment. Asterisks represent significant differences in survival between treatments (*$p < 0.05$; **$p < 0.001$, $n = 30$). **(C)** The viral genome copy number and infection prevalence of CHIKV were measured 14 days after an infected blood meal challenge ($n = 30$). qRT-PCR was used to assess genome copy number and infection prevalence in individual mosquitoes, with each dot representing the viral load from individual mosquitoes. Each pie chart indicates the percentage of mosquitos that died by day 5 (in red), that are alive but with lower virus level of $\leq 10^2$ (blue), or that have an high virus level (black). Lines A and B represent different CasRx lines (Supplementary Table S2). Horizontal red lines indicate the median of the viral loads. Considering the non-normal distribution of viral titers, the median was used to describe central tendency. The nonparametric Mann–Whitney test was used to compare median viral titers, and Fisher's exact test was used to compare infection prevalence. *$p < 0.05$, **$p < 0.01$, $n = 30$. qRT-PCR, real-time quantitative reverse transcription PCR; REAPER, vRNA Expression Activates Poisonous Effector Ribonuclease.

The confirmation of collateral activity has been observed in Cas13 proteins *in vitro*,[16,17,25,44] and it has been effectively employed for the sensitive detection of nucleic acids.[45] However, with the controversial nature of CasRx, comprehensive studies are needed that could improve Cas-based Trojan horse systems and other applications that exploit collateral activity in depth.

The presented design of the REAPER system lays out a foundational technology that can be further optimized and expanded. In the initial designs, we compared the expression of CasRx fused with either an NLS or NES and found no considerable differences in activity against two phenotypic genes. Nonetheless, the NES is critical for targeting viruses, which replicate in the cytoplasm (Fig. 4; Supplementary Fig. S6).

This points out that the subcellular localization of a target will be an important factor to consider when designing a REAPER strategy in other organisms. We also observed transcriptome misregulation when expressing CasRx alone with a ubiquitin promoter, which may lead to toxicity, limit fitness, or reduce the efficacy of an antiviral platform. Future designs should, therefore, implement tissue-specific or inducible promoters for CasRx expression to reduce the deleterious effects associated with ubiquitous expression.

Furthermore, gRNA design and *in vitro* screening are likely to enhance the potency of the REAPER system, exemplified through our analysis using the SENSR system (Fig. 3). In this study, we targeted four conserved regions of CHIKV *nsp* genes.[41] However, further screening may identify gRNA targets with improved cutting efficiency or less evolutionary constraints on virus replication. For example, by targeting conserved noncoding regions, there is potential to bypass the region prone to virus mutation and avoid the risk of sparing crucial regulatory elements necessary for virus replication and survival.

However, it is important to note that noncoding regions of viruses tend to be highly structured, and targeting them with CRISPR-Cas systems may be challenging due to limited accessibility to the target site. In addition, targeting noncoding regions could potentially have unintended effects on host gene expression or regulatory mechanisms, which would require careful evaluation and monitoring. Overall, further research is needed to determine the feasibility and potential effectiveness of targeting conserved noncoding regions of viruses for antiviral purposes. Our results also demonstrate that multiplexed gRNAs are functional in the system (Fig. 4), which can permit the generation of future multi-virus antiviral systems.

Our strategy, combined with gene drive technology, can minimize or eliminate the risk of CHIKV transmission by mosquitoes. Gene drive is a method used to spread a specific genetic trait throughout a population by ensuring that the trait is inherited more frequently than usual.[46] Effective Cas9-mediated homing-based gene drives have been demonstrated in malaria vectors[47,48] and *Ae. Aegypti*,[14] indicating their potential for controlling the transmission of diseases.

By linking our REAPER technology to a gene drive system, it is possible to rapidly convert wild mosquito populations into transgenic homozygotes that are resistant to CHIKV transmission. However, it is important to note that gene drive technology regulation varies worldwide, with some countries having established rules, whereas others are developing them. The World Health Organization has issued guidelines for responsible gene drive technology use in insect-borne disease control, encompassing safety, ethics, and community involvement. Overall, the regulation of gene drive technology is a constantly evolving field that will likely continue to develop as new applications are developed and tested.

Overall, our results with the REAPER system indicate that CasRx can be used to engineer interference against RNA viruses in mosquitoes. Correspondingly, finding or engineering novel CRISPR ribonucleases with increased collateral activity or understanding how collateral activity is triggered by different gRNAs sequences will be very important to improve the REAPER technology. Maximizing the speed and robustness of REAPER will lead to the generation of novel mechanisms for RNA-guided immunity against multiple diseases in vertebrates and provides a platform to develop novel mosquito control strategies for arboviruses.

Acknowledgment

We thank Judy Ishikawa for mosquito husbandry assistance.

Authors' Contributions

O.S.A., P.N.P., and E.D.B. conceived and designed the experiments. E.D.B., H.-H.L., R.A.M., A.J.L.-D., D.J.B., M.B., T.Y., M.L., and I.A. performed molecular and genetic experiments. I.A. performed the RNA sequencing experiments and analysis. A.J.L.-D., M.D., M.J.K., S.J., K.C., and K.R.B. performed viral infection experiments and analysis. All authors contributed to the writing, analyzed the data, and approved the final article.

Ethical Conduct of Research

All animals were handled in accordance with the Guide for the Care and Use of Laboratory Animals as recommended by the National Institutes of Health and approved by the UCSD Institutional Animal Care and Use Committee (IACUC, Animal Use Protocol #S17187) and UCSD Biological Use Authorization (BUA #R2401).

Data Availability

All plasmids and annotated DNA sequence maps are available at www.addgene.com under accession numbers 191374 (OA-1050T), 191375 (OA-1085F), 191376 (OA-1085L), 194001 (OA-1163A), and 194003 (OA-1093B). Raw sequencing data are available at NCBI Sequence Read Archive (SRA), accession number PRJNA912231 (reviewer link: https://dataview.ncbi.nlm.nih.gov/object/PRJNA912231?reviewer=7ll0k7o7hauq2eh8kbv16mjbj9).

Author Disclosure Statement

O.S.A. is a founder of both Agragene, Inc. and Synvect, Inc., with equity interest. The terms of this arrangement have been reviewed and approved by the University of California, San Diego in accordance with its conflict of interest policies. L.A is an adviser to Synvect, Inc. and Biocentis Ltd., with financial interest in both. All other authors declare no competing interests.

Funding Information

This study was supported by funding from NIH awards (R01AI151004, R01GM132825, RO1AI148300, RO1AI175152, DP2AI152071, and R21AI149161), EPA STAR award (RD84020401), and an Open Philanthropy award (309937-0001) awarded to O.S.A. We acknowledge the capabilities of the Australian Centre for Disease Preparedness (grid.413322.5) in undertaking

this research, including infrastructure funded by the National Collaborative Research Infrastructure Strategy. Figures were created by BioRender.com

Supplementary Material

Supplementary Figure S1
Supplementary Figure S2
Supplementary Figure S3
Supplementary Figure S4
Supplementary Figure S5
Supplementary Figure S6
Supplementary Figure S7
Supplementary Figure S8
Supplementary Table S1
Supplementary Table S2
Supplementary Table S3
Supplementary Table S4
Supplementary Table S5
Supplementary Table S6
Supplementary Table S7
Supplementary Table S8
Supplementary Table S9
Supplementary Table S10
Supplementary Table S11
Supplementary Table S12
Supplementary Table S13
Supplementary Table S14
Supplementary Table S15
Supplementary Table S16
Supplementary Table S17
Supplementary Table S18
Supplementary Table S19
Supplementary Table S20
Supplementary Table S21

References

1. Weaver SC, Reisen WK. Present and future arboviral threats. Antiviral Res 2010;85(2):328–345.
2. Achee NL, Grieco JP, Vatandoost H, et al. Correction: Alternative strategies for mosquito-borne arbovirus control. PLoS Negl Trop Dis 2019;13(3): e0007275.
3. Dusfour I, Vontas J, David J-P, et al. Management of insecticide resistance in the major Aedes vectors of arboviruses: Advances and challenges. PLoS Negl Trop Dis 2019;13(10):e0007615.
4. Baca A, Gundacker N, Sanchez JL. 2774. Impact of yellow fever vaccine and recombinant zoster vaccine shortages on patients presenting to a Travel Clinic. Open Forum Infect Dis 2019;6(Supplement_2):S979; doi: 10.1093/ofid/ofz360.2451
5. Lucey DR, Donaldson H. Yellow fever vaccine shortages in the United States and abroad: A critical issue. Ann Intern Med 2017;167(9):664; doi: 10.7326/m17-1337
6. Abbink P, Larocca RA, De La Barrera RA, et al. Protective efficacy of multiple vaccine platforms against Zika virus challenge in rhesus monkeys. Science 2016;353(6304):1129–1132.
7. Halstead SB. Dengvaxia sensitizes seronegatives to vaccine enhanced disease regardless of age. Vaccine 2017;35(47):6355–6358.
8. Powers AM. Vaccine and therapeutic options to control Chikungunya Virus. Clin Microbiol Rev 2018;31(1):e00104-16; doi: 10.1128/CMR .00104-16
9. Norton SA, Morens DM. Vaccination strategies during shortages of yellow fever vaccine. JAMA 2018;319(12):1280; doi: 10.1001/jama.2018.0200
10. Buchman A, Gamez S, Li M, et al. Broad dengue neutralization in mosquitoes expressing an engineered antibody. PLoS Pathog 2020;16(1): e1008103.
11. Buchman A, Gamez S, Li M, et al. Engineered resistance to Zika virus in transgenic *Aedes Aegypti* expressing a polycistronic cluster of synthetic small RNAs. Proc Natl Acad Sci 2019;116(9):3656–3661; doi: 10.1073/pnas.1810771116
12. Liu W-L, Hsu C-W, Chan S-P, et al. Author correction: Transgenic refractory Aedes aegypti lines are resistant to multiple serotypes of dengue virus. Sci Rep 2022;12(1):754.
13. Li M, Yang T, Bui M, et al. Suppressing mosquito populations with precision guided sterile males. Nat Commun 2021;12(1):5374.
14. Li M, Yang T, Kandul NP, et al. Development of a Confinable Gene Drive System in the human disease vector Aedes aegypti. eLife 2020;9: e51701; doi: 10.7554/elife.51701
15. Verkuijl SAN, Gonzalez E, Li M, et al. A CRISPR endonuclease gene drive reveals distinct mechanisms of inheritance bias. Nat Commun 2022; 13(1):7145; doi: 10.1038/s41467-022-34739-y
16. Abudayyeh OO, Gootenberg JS, Essletzbichler P, et al. RNA targeting with CRISPR-Cas13. Nature 2017;550(7675):280–284.
17. Konermann S, Lotfy P, Brideau NJ, et al. Transcriptome engineering with RNA-targeting type VI-D CRISPR effectors. Cell 2018;173(3):665–676.e14.
18. Kushawah G, Hernandez-Huertas L, Abugattas-Nuñez Del Prado J, et al. CRISPR-Cas13d induces efficient mRNA knockdown in animal embryos. Dev Cell 2020;54(6):805–817.e7.
19. Li J, Zhu D, Hu S, et al. CRISPR-CasRx knock-in mice for RNA degradation. Sci China Life Sci 2022;65:2248–2256; doi: 10.1007/s11427-021-2059-5
20. Buchman AB, Brogan DJ, Sun R, et al. Programmable RNA targeting using CasRx in flies. CRISPR J 2020;3(3):164–176.
21. Sun R, Brogan D, Buchman A, et al. Ubiquitous and tissue-specific RNA targeting in Drosophila Melanogaster using CRISPR/CasRx. J Vis Exp 2021;(168); doi: 10.3791/62154
22. Aman R, Ali Z, Butt H, et al. RNA virus interference via CRISPR/Cas13a system in plants. Genome Biol 2018;19(1):1.
23. Bot JF, van der Oost J, Geijsen N. The double life of CRISPR–Cas13. Curr Opin Biotechnol 2022;78:102789; doi: 10.1016/j.copbio.2022.102789
24. Li Y, Xu J, Guo X, et al. The collateral activity of RfxCas13d can induce lethality in a RfxCas13d knock-in mouse model. Genome Biol 2023; 24(1):20.
25. Abudayyeh OO, Gootenberg JS, Konermann S, et al. C2c2 is a single-component programmable RNA-guided RNA-targeting CRISPR effector. Science 2016;353(6299):aaf5573.
26. van den Hurk AF, Hall-Mendelin S, Webb CE, et al. Role of enhanced vector transmission of a new West Nile virus strain in an outbreak of equine disease in Australia in 2011. Parasit Vectors 2014;7(1):1–10.
27. Carrington LB, Simmons CP. Human to mosquito transmission of dengue viruses. Front Immunol 2014;5:290.
28. Morgan P. Kain BMB. Can existing data on West Nile virus infection in birds and mosquitos explain strain replacement? Ecosphere n.d.;8(3): 1–18.
29. Lequime S, Dehecq J-S, Matheus S, et al. Modeling intra-mosquito dynamics of Zika virus and its dose-dependence confirms the low epidemic potential of Aedes albopictus. PLoS Pathog 2020;16(12): e1009068.
30. Tjaden NB, Thomas SM, Fischer D, et al. Extrinsic incubation period of dengue: Knowledge, backlog, and applications of temperature dependence. PLoS Negl Trop Dis 2013;7(6):e2207.
31. Brogan DJ, Chaverra-Rodriguez D, Lin CP, et al. Development of a rapid and sensitive CasRx-based diagnostic assay for SARS-CoV-2. ACS Sens 2021;6(11):3957–3966.
32. Bui M, Li M, Raban RR, et al. Embryo microinjection techniques for efficient site-specific mutagenesis in Culex quinquefasciatus. J Vis Exp 2020;(159); doi: 10.3791/61375.
33. Sun R, Li M, McMeniman CJ, et al. CRISPR-mediated genome engineering in Aedes aegypti. Methods Mol Biol 2022;2509:23–51.
34. Dzaki N, Ramli KN, Azlan A, et al. Evaluation of reference genes at different developmental stages for quantitative real-time PCR in Aedes aegypti. Sci Rep 2017;7:43618.
35. Dobin A, Davis CA, Schlesinger F, et al. STAR: Ultrafast universal RNA-seq aligner. Bioinformatics 2013;29(1):15–21.
36. Brieba LG, Padilla R, Sousa R. Role of T7 RNA polymerase His784 in start site selection and initial transcription. Biochemistry 2002;41(16):5144–5149.

37. Vedururu RK, Neave MJ, Tachedjian M, et al. RNASeq analysis of Aedes Albopictus Mosquito midguts after Chikungunya virus infection. Viruses 2019;11(6):513; doi: 10.3390/v11060513
38. Anderson MAE, Gross TL, Myles KM, et al. Validation of novel promoter sequences derived from two endogenous ubiquitin genes in transgenic Aedes aegypti. Insect Mol Biol 2010;19(4):441–449.
39. Li M, Yang T, Kandul NP, et al. Development of a confinable gene drive system in the human disease vector. Elife 2020;9:e51701; doi: 10.7554/eLife.51701
40. Li M, Bui M, Yang T, et al. Germline Cas9 expression yields highly efficient genome engineering in a major worldwide disease vector, *Aedes Aegypti*. Proc Natl Acad Sci 2017;114(49):E10540–E10549; doi: 10.1073/pnas.1711538114
41. Tng PYL, Carabajal Paladino LZ, Anderson MAE, et al. Intron-derived small RNAs for silencing viral RNAs in mosquito cells. PLoS Negl Trop Dis 2022;16(6):e0010548.
42. Mahas A, Aman R, Mahfouz M. CRISPR-Cas13d mediates robust RNA virus interference in plants. Genome Biol 2019;20(1):263.
43. Wang Q, Liu Y, Han C, et al. Efficient RNA virus targeting via CRISPR/CasRx in fish. J Virol 2021;95(19):e0046121; doi: 10.1128/jvi.00461-21
44. East-Seletsky A, O'Connell MR, Knight SC, et al. Two distinct RNase activities of CRISPR-C2c2 enable guide-RNA processing and RNA detection. Nature 2016;538(7624):270–273.
45. Gootenberg JS, Abudayyeh OO, Lee JW, et al. Nucleic acid detection with CRISPR-Cas13a/C2c2. Science 2017;356(6336):438–442.
46. Champer J, Buchman A, Akbari OS. Cheating evolution: Engineering gene drives to manipulate the fate of wild populations. Nat Rev Genet 2016;17(3):146–159.
47. Gantz VM, Jasinskiene N, Tatarenkova O, et al. Highly efficient Cas9-mediated gene drive for population modification of the malaria vector mosquito Anopheles stephensi. Proc Natl Acad Sci U S A 2015;112(49):E6736–E6743.
48. Hammond A, Galizi R, Kyrou K, et al. A CRISPR-Cas9 gene drive system targeting female reproduction in the malaria mosquito vector Anopheles gambiae. Nat Biotechnol 2016;34(1):78–83.

Received: August 26, 2023
Accepted: November 14, 2023
Online Publication Date: December 8, 2023